Steel and Composite Structures, *Vol. 20, No. 4 (2016) 889-911*
DOI: http://dx.doi.org/10.12989/scs.2016.20.4.889

Mechanical and hygrothermal behaviour of functionally graded plates using a hyperbolic shear deformation theory

Imene Laoufi [1], Mohammed Ameur [*1,2], Mohamed Zidi [1,3], El Abbes Adda Bedia [1,3] and Abdelmoumen Anis Bousahla [1]

[1] *Laboratoire des Matériaux et Hydrologie*, *Université de Sidi Bel Abbes*, *BP 89 Cité Ben M'hidi 22000 Sidi Bel Abbes*, *Algérie*
[2] *Département de génie civil*, *Ecole Nationale Polytechnique d'Oran*, *Algérie*
[3] *Département de génie civil*, *Faculté des Sciences de l'Ingénieur*, *Université Sidi Bel Abbes*, *Algérie*

(*Received August 17, 2015, Revised December 16, 2015, Accepted December 21, 2015*)

Abstract. Using the hyperbolic shear deformation plate model and including plate-foundation interaction (Winkler and Pasternak model), an analytical method in order to determine the deflection and stress distributions in simply supported rectangular functionally graded plates (FGP) subjected to a sinusoidal load, a temperature and moisture fields. The present theory exactly satisfies stress boundary conditions on the top and the bottom of the plate. No transversal shear correction factors are needed because a correct representation of the transversal shearing strain is given. Materials properties of the plate (elastic, thermal and moisture expansion coefficients) are assumed to be graded in the thickness direction according to a simple power-law distribution in terms of the volume fractions of the constituents. Numerical examples are presented and discussed for verifying the accuracy of the present theory in predicting the bending response of FGM plates under sinusoidal load and a temperature field as well as moisture concentration. The effects of material properties, temperature, moisture, plate aspect ratio, side-to-thickness ratio, ratio of elastic coefficients (ceramic-metal) and three distributions for both temperature and moisture on deflections and stresses are investigated.

Keywords: FG plates; elastic foundation; hyperbolic shear deformation; hygro-thermal load

1. Introduction

The idea of a functionally graded material is not a new one. Examples of functionally graded materials are evident in nature: bone, shell, balsa wood and bamboo all have their greatest strength on the outside, where the greatest protection is required (Suresh and Mortensen 1998). However it was not until the 1980's in Japan that the idea of a functionally graded material was actively researched in order to gain advances in high temperature aerospace applications (Koizumi 1993). Since then, functionally graded materials have usually been designed specifically for their application. The FGM is suitable for various applications, such as thermal coatings of barrier for ceramic engines, gas turbines, nuclear fusions, optical thin layers, biomaterial electronics, etc. The material properties of the FGMs vary continuously from one interface to the other in the thickness

*Corresponding author, Doctor, E-mail: mohammed.ameur@gmail.com

http://www.techno-press.org/?journal=scs&subpage=6 ISSN: 1229-9367 (Print), 1598-6233 (Online)

direction (Javaheri and Eslami 2002). These structures possess advantages of high modulus, high strength and low weight without stress concentration or delamination in composite materials.

Rectangular plates made of FGMs are often employed as a part of engineering structures. Such plate structures can be found in various kinds of industrial applications like raft foundations, storage tanks, swimming pools, and in most civil engineering constructions. One and two parameter models for the soil underneath the plate are introduced to model the foundation.

Liu and his co-workers (Tani and Liu 1993, Liu and Tani 1994, Liu *et al*. 1999, 2001, 2003, Dai *et al*. 2005) gave a good review part of the history on simulation of FGM structures. Their superior strength and stiffness properties, however, are often compromised by the environment to which they are exposed. A general discussion of the effect of environment on the structural behavior of FGM materials has been presented by many researchers.

As an elevation of temperature and moisture concentrations, the elastic moduli and the strength of FGMs will degrade. The deformation and stress analysis of different plate structures subjected to moisture and temperature has been the subject of research interest of many investigators (Whitney and Ashton 1971, Patel *et al*. 2002, Bahrami and Nosier 2007, Benkhedda *et al*. 2008, Lo *et al*. 2010, Shen 2001, Rao and Sinha 2004, Wang *et al*. 2005, Lo *et al*. 2010, Zenkour 2010).

Recently, a new four variable refined plate theory which involves only four unknown functions and yet takes into account shear deformations has been developed by Tounsi and co-workers (Benachour *et al*. 2011) for free vibration analysis, (Bourada *et al*. 2012, Khalfi *et al*. 2014 and Ait Amar Meziane *et al*. 2014) for buckling and free vibration analysis, (Tounsi *et al*. 2013, and Houari *et al*. 2013) for thermoelastic bending analysis, (Said *et al*. 2014, Bourada *et al*. 2015 and Belabed *et al*. 2014) for new shear deformation theory, (Zidi *et al*. 2014 and Bousahla *et al*. 2014) for bending analysis, (Bouchafa *et al*. 2015) thermal stresses and deflections analysis, (Bessaim *et al*. 2013, Mahi *et al*. 2015 and Hebali *et al*. 2014), for bending and free vibration analysis, (Ait Atmane *et al*. 2016) for study effect of thickness stretching and porosity on mechanical response, (Ait Yahia 2015) for wave propagation in FG plates with porosities using various higher-order shear deformation plate theories. This four variable refined plate theory is based on the assumption that the in-plane and transverse displacements consist of bending and shear components in which the bending components do not contribute toward shear forces and, likewise, the shear components do not contribute toward bending moments. The most interesting feature of this theory is that it accounts for a quadratic variation of the transverse shear strains across the thickness, and satisfies the zero traction boundary conditions on the top and bottom surfaces of the plate without using shear correction factors. Other researchers (Hamidi *et al*. 2015, Fekrar *et al*. 2014, Zenkour 2006 and Benoun *et al*. 2016) developed their works by using high order shear deformation theories with five variables. From the literature reviewed, it can be found that research on mechanical and hygrothermal behaviour of functionally graded plates using a hyperbolic deformation theory seems to be lacking, which is the problem to be addressed in this paper.

The objective of this investigation is to present a general hygrothermal formulation for FGM rectangular plates using the hyperbolic shear deformation theory (Said *et al*. 2014).

Therefore, the aim of this study is to extend the four variable refined plate theory to the hygro-thermo-mechanical bending behavior of FGM rectangular plate. The elastic, thermal and moisture expansion coefficients of the plate are assumed to be graded in the thickness direction. The influences played by many parameters such as transversal shear deformation, plate aspect ratio, side-to-thickness ratio, volume fraction distributions, moisture concentration, and elastic foundation parameters on the structural response are investigated in detail.

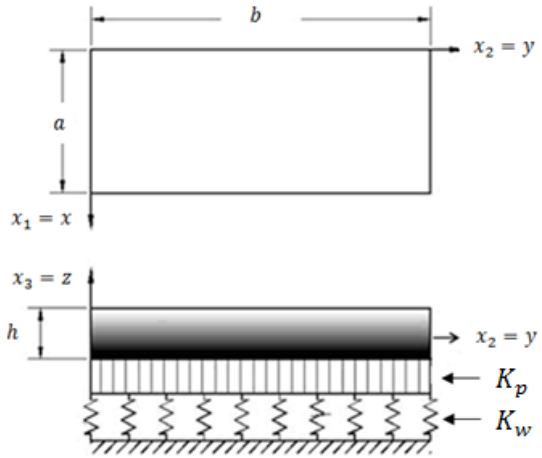

Fig. 1 Configuration of rectangular FGM plate resting on elastic foundation

2. Mathematical model and governing equations

In this study, rectangular functionally graded plate having sides $a \times b$ and thickness h, referred to the rectangular Cartesian coordinates (x_1, x_2, x_3), where (x_1, x_2) plane coincides with middle surface of the plate and (x_3) is the thickness coordinate $(-h/2 \leq x_3 \leq h/2)$, as shown in Fig. 1, are considered. The FGM plate is subjected to a transverse load $q(x_1, x_2)$. The material properties of the plate are assumed to vary through the thickness of the plate with a desired variation of the volume fractions of two materials in between the two surfaces. By applying a simple power law distribution, the volume fractions of metal and ceramic are expressed as (Zenkour 2006)

$$V_c(x_3) = \left(\frac{x_3}{h} + \frac{1}{2}\right)^k \quad (0 \leq k < \infty), \quad V_c(x_3) + V_m(x_3) = 1 \tag{1}$$

Where V, the superscript p, the subscripts c and m represent the volume fraction, the volume fraction index, ceramic and metal, respectively.

2.1 Assumptions

Assumptions of the hyperbolic shear deformation theory (Said *et al*. 2014) are as follows:

(1) The origin of the Cartesian coordinate system is taken at the neutral surface of the FGM plate.
(2) The displacements are small in comparison with the plate thickness and, therefore, strains involved are infinitesimal.
(3) The transverse displacement w includes two components of bending w_b, and shear w_s. These components are functions of coordinates x_1, x_2 only

$$u_3(x_1, x_2, x_3) = w_b(x_1, x_2) + w_s(x_1, x_2) \tag{2}$$

(4) The transverse normal stress S_{33} is negligible in comparison with in-plane stresses S_{11} and S_{22}.

(5) The displacements u_1 in x_1-direction and u_2 in x_2-direction consist of extension, bending, and shear components.

$$u_1 = u + u_b + u_s\,,\quad u_2 = v + v_b + v_s \tag{3}$$

The bending components u_b and v_b are assumed to be similar to the displacements given by the classical plate theory. Therefore, the expression for u_b and v_b can be given as

$$u_b = -x_3\, w_{b\,,x_1}\,,\quad v_b = -x_3\, w_{b\,,x_2} \tag{4}$$

The shear components u_s and v_s give rise, in conjunction with w_s, to the parabolic variations of shear strains γ_{13}, γ_{23} and hence to shear stresses S_{13}, S_{23} through the thickness of the plate in such a way that shear stresses S_{13}, S_{23} are zero at the top and bottom faces of the plate. Consequently, the expression for u_s and v_s can be given as

$$u_s = -f(x_3)\, w_{s\,,x_1}\,,\quad v_s = -f(x_3)\, w_{s\,,x_2} \tag{5}$$

2.2 Kinematics

According to the preceding assumptions, the displacements of a material point located at (x_1, x_2, x_3) in the FGM plate may be written as follows

$$\left.\begin{aligned} u_1(x_1,x_2,x_3) &= u(x_1,x_2) - x_3\, w_{b\,,x_1} + f(x_3)\phi_1\,,\\ u_2(x_1,x_2,x_3) &= v(x_1,x_2) - x_3\, w_{b\,,x_2} + f(x_3)\phi_2\,,\\ u_3(x_1,x_2,x_3) &= w_b(x_1,x_2) + w_s(x_1,x_2). \end{aligned}\right\} \tag{6}$$

Where u and v are the mid-plane displacements of the plate in the x_1 and x_2 direction, respectively; w_b and w_s are the bending and shear components of transverse displacement, respectively.

And

$$\phi_1 = w_{s,x_1},\quad \phi_2 = w_{s,x_2} \tag{7}$$

$(\ )_{,x_1}$ and $(\ )_{,x_2}$ are partial derivative with respect to x_1 and x_2, respectively.

Under this assumptions, the strain field associated with the displacements in Eq. (6) are

$$\left.\begin{aligned} \begin{Bmatrix}\varepsilon_{11}\\ \varepsilon_{22}\\ \gamma_{12}\end{Bmatrix} &= \begin{Bmatrix}\varepsilon^0_{11}\\ \varepsilon^0_{22}\\ \gamma^0_{12}\end{Bmatrix} + x_3\begin{Bmatrix}\kappa^b_1\\ \kappa^b_2\\ \kappa^b_{12}\end{Bmatrix} + f(x_3)\begin{Bmatrix}\kappa^s_1\\ \kappa^s_2\\ \kappa^s_{12}\end{Bmatrix},\\ \begin{Bmatrix}\gamma_{23}\\ \gamma_{13}\end{Bmatrix} &= g(x_3)\begin{Bmatrix}\gamma^s_{23}\\ \gamma^s_{13}\end{Bmatrix} \end{aligned}\right. \tag{8}$$

Where

$$\begin{Bmatrix}\varepsilon^0_{11}\\ \varepsilon^0_{22}\\ \gamma^0_{12}\end{Bmatrix} = \begin{Bmatrix} u_{,x_1}\\ v_{,x_2}\\ u_{,x_2} + v_{,x_1}\end{Bmatrix},\quad \begin{Bmatrix}\kappa^b_1\\ \kappa^b_2\\ \kappa^b_{12}\end{Bmatrix} = \begin{Bmatrix} -w_{b,,x_1}\\ -w_{b,,x_2}\\ -2w_{b,x_1x_2}\end{Bmatrix} \tag{9a}$$

$$\begin{Bmatrix} \kappa_1^s \\ \kappa_2^s \\ \kappa_{12}^s \end{Bmatrix} = \begin{Bmatrix} -w_{s,,x_1} \\ -w_{s,,x_2} \\ -2w_{s,x_1 x_2} \end{Bmatrix}, \quad \begin{Bmatrix} \gamma_{23}^s \\ \gamma_{13}^s \end{Bmatrix} = \begin{Bmatrix} w_{s,,x_2} \\ w_{s,,x_1} \end{Bmatrix} \tag{9b}$$

and

$$f(x_3) = \frac{(h/\pi)sinh\left(\frac{\pi}{h}x_3\right) - x_3}{cosh(\pi/2) - 1}, \quad g(x_3) = 1 - f(x_3)_{,x_3} \tag{10}$$

2.3 Constitutive equations

The stress-strain relationships can be expressed as

$$\begin{Bmatrix} S_{11} \\ S_{22} \end{Bmatrix} = \frac{E(z)}{1-\nu^2}\begin{bmatrix} 1 & \nu \\ \nu & 1 \end{bmatrix}\begin{Bmatrix} \varepsilon_{11-\alpha\Delta T-\beta\Delta C} \\ \varepsilon_{22-\alpha\Delta T-\beta\Delta C} \end{Bmatrix},$$
$$\{S_{12},\ S_{23},\ S_{31}\} = \frac{E(z)}{2(1+\nu)}\{\gamma_{12},\ \gamma_{23},\ \gamma_{31}\}. \tag{11}$$

Where$(S_{11},\ S_{22},\ S_{12},\ S_{23},\ S_{31})and\left(\varepsilon_{11},\ \varepsilon_{22},\ \gamma_{12},\ \gamma_{23},\ \gamma_{31}\right)$are the stress and strain components, respectively. Where α and β are thermal and moisture expansion coefficients.

Where $\Delta T = T - T_0$ and $\Delta C = C - C_0$ are the difference of temperature and moisture content respectively and in which T_0 is the reference temperature, C_0 is the reference moisture concentration, T is the applied temperature and C is moisture concentration.

The applied temperature distribution $T(x_1, x_2, x_3)$ and the moisture concentration $C(x_1, x_2, x_3)$ through the thickness are assumed, respectively (Bouderba *et al*. 2013)

$$\left.\begin{aligned} T(x_1, x_2, x_3) &= T_1(x_1, x_2) + \frac{x_3}{h}T_2(x_1, x_2) + \frac{1}{h}\,\Psi(x_3)\,T_3(x_1, x_2) \\ C(x_1, x_2, x_3) &= C_1(x_1, x_2) + \frac{x_3}{h}C_2(x_1, x_2) + \frac{1}{h}\,\Psi(x_3)\,C_3(x_1, x_2) \end{aligned}\right\} \tag{12}$$

2.4 Governing equations

The principle of virtual displacements is used herein to derive the governing equations. The principle can be stated in an analytical form as

$$0 = \int_A \int_{-h/2}^{h/2} \left[S_{11}\delta\varepsilon_1 + S_{22}\delta\varepsilon_2 + S_{12}\delta\gamma_{12} + S_{23}\delta\gamma_{23} + S_{13}\delta\gamma_{13}\right] dx_3 dA - \int_A (q - f_e)\,\delta u_3 dA$$

$$\begin{aligned} 0 = \int_A \big[&N_1\delta\varepsilon_{11}^0 + N_2\delta\varepsilon_{22}^0 + N_{12}\delta\varepsilon_{12}^0 + M_1^b\delta k_1^b + M_2^b\delta k_2^b + M_{12}^b\delta k_{12}^b \\ &+ M_1^s\delta k_1^s + M_2^s\delta k_2^s + M_{12}^s\delta k_{12}^s + S_{23}^s\delta\gamma_{23}^s + S_{13}^s\delta\gamma_{13}^s\big]dA \\ &- \int_A (q - f_e)\,(\delta w_b + \delta w_s)dA \end{aligned} \tag{13}$$

Where S_{ij} is the Cauchy stress tensor, ε_{ij} is the small strain tensor, q is the transverse load; and N, M and S are the stress and moment resultants of the FGM plate.

The bottom surface of the plate is assumed subjected to Winkler–Pasternak elastic foundation (see Fig. 1), the reaction–deflection relation at the bottom surface of the model is expressed by

$$f_e = K_w u_3 - K_{px_1} u_{3,,x_1} - K_{px_2} u_{3,,x_2}. \tag{14}$$

Where f_e is the density of reaction force of foundation. K_w is the modulus of subgrade reaction (elastic coefficient of the foundation) and K_{px_1} and K_{px_2} are the shear moduli of the subgrade (shear layer foundation stiffness). If foundation is homogeneous and isotropic, we will get $K_{px_1} = K_{px_2} = K_p$. If the shear layer foundation stiffness is neglected, Pasternak foundation becomes a Winkler foundation.

The stress resultants N, M, and S are defined by

$$\begin{Bmatrix} N_1, & N_2, & N_{12} \\ M_1^b, & M_2^b, & M_{12}^b \\ M_1^s, & M_2^s, & M_{12}^s \end{Bmatrix} = \int_{-h/2}^{h/2} (S_{11}, S_{22}, S_{12}) \begin{Bmatrix} 1 \\ x_3 \\ f(x_3) \end{Bmatrix} dx_3, \tag{15a}$$

$$(Q_{13}^s,\ Q_{23}^s) = \int_{-h/2}^{h/2} (S_{13},\ S_{23})\, g(x_3) dx_3. \tag{15b}$$

Substituting Eq. (5) into Eq. (11) and integrating through the thickness of the plate, the stress resultants are given as

$$\begin{Bmatrix} N_1 \\ N_2 \\ N_{12} \\ M_1^b \\ M_2^b \\ M_{12}^b \\ M_1^s \\ M_2^s \\ M_{12}^s \end{Bmatrix} = \begin{bmatrix} A_{11} & A_{12} & 0 & B_{11} & B_{12} & 0 & B_{11}^s & B_{12}^s & 0 \\ A_{12} & A_{22} & 0 & B_{12} & B_{22} & 0 & B_{12}^s & B_{22}^s & 0 \\ 0 & 0 & A_{66} & 0 & 0 & B_{66} & 0 & 0 & B_{66}^s \\ B_{11} & B_{12} & 0 & D_{11} & D_{12} & 0 & D_{11}^s & D_{12}^s & 0 \\ B_{12} & B_{22} & 0 & D_{12} & D_{22} & 0 & D_{12}^s & D_{22}^s & 0 \\ 0 & 0 & B_{66} & 0 & 0 & D_{66} & 0 & 0 & D_{66}^s \\ B_{11}^s & B_{12}^s & 0 & D_{11}^s & D_{12}^s & 0 & H_{11}^s & H_{12}^s & 0 \\ B_{12}^s & B_{22}^s & 0 & D_{12}^s & D_{22}^s & 0 & H_{12}^s & H_{22}^s & 0 \\ 0 & 0 & B_{66}^s & 0 & 0 & D_{66}^s & 0 & 0 & H_{66}^s \end{bmatrix} \begin{Bmatrix} \varepsilon_1^0 \\ \varepsilon_2^0 \\ \gamma_{12}^0 \\ \kappa_1^b \\ \kappa_2^b \\ \kappa_{12}^b \\ \kappa_1^s \\ \kappa_2^s \\ \kappa_{12}^s \end{Bmatrix} - \begin{Bmatrix} N_1^T \\ N_2^T \\ 0 \\ M_1^{bT} \\ M_2^{bT} \\ 0 \\ M_1^{sT} \\ M_2^{sT} \\ 0 \end{Bmatrix} - \begin{Bmatrix} N_1^C \\ N_2^C \\ 0 \\ M_1^{bC} \\ M_2^{bC} \\ 0 \\ M_1^{sC} \\ M_2^{sC} \\ 0 \end{Bmatrix}, \tag{16a}$$

$$\begin{Bmatrix} Q_{23}^s \\ Q_{13}^s \end{Bmatrix} = \begin{bmatrix} A_{44}^s & 0 \\ 0 & A_{55}^s \end{bmatrix} \begin{Bmatrix} \gamma_{23} \\ \gamma_{13} \end{Bmatrix}, \tag{16b}$$

Where A_{ij}, B_{ij}, etc., are the plate stiffness, defined by

$$\begin{Bmatrix} A_{11} & B_{11} & D_{11} & B_{11}^s & D_{11}^s & H_{11}^s \\ A_{12} & B_{12} & D_{12} & B_{12}^s & D_{12}^s & H_{12}^s \\ A_{66} & B_{66} & D_{66} & B_{66}^s & D_{66}^s & H_{66}^s \end{Bmatrix} = \tag{17a}$$

$$\int_{-h/2}^{h/2} \frac{E(x_3)}{1-\nu^2}\left(1,\ x_3,\ x_3^2, f(x_3),\ x_3 f(x_3),\ f^2(x_3)\right)\begin{Bmatrix} 1 \\ \nu \\ \dfrac{1-\nu}{2} \end{Bmatrix} dx_3, \tag{17a}$$

$$(A_{22},\ B_{22},\ D_{22},\ B_{22}^s,\ D_{22}^s,\ H_{22}^s) = (A_{11},\ B_{11},\ D_{11},\ B_{11}^s,\ D_{11}^s,\ H_{11}^s), \tag{17b}$$

$$A_{44}^s = A_{55}^s = \int_{-h/2}^{h/2} \frac{E(x_3)}{2(1-\nu)}[g(x_3)]^2 dx_3, \tag{17c}$$

The stress and moment resultants due to thermal and hygroscopic loading are defined respectively by

$$\begin{Bmatrix} N_1^T \\ M_1^{bT} \\ M_1^{sT} \end{Bmatrix} = \begin{Bmatrix} N_2^T \\ M_2^{bT} \\ M_2^{sT} \end{Bmatrix} = \int_{-h/2}^{h/2} \frac{E(x_3)}{1-\nu}\alpha(x_3)T\begin{Bmatrix} 1 \\ x_3 \\ f(x_3) \end{Bmatrix} dx_3, \tag{18a}$$

$$\begin{Bmatrix} N_1^C \\ M_1^{bC} \\ M_1^{sC} \end{Bmatrix} = \begin{Bmatrix} N_2^C \\ M_2^{bC} \\ M_2^{sC} \end{Bmatrix} = \int_{-h/2}^{h/2} \frac{E(x_3)}{1-\nu}\beta(x_3)C\begin{Bmatrix} 1 \\ x_3 \\ f(x_3) \end{Bmatrix} dx_3, \tag{18b}$$

Integrating the expressions in Eq. (13) by parts and collecting the coefficients of δu, δv, δw_b, and δw_s, one obtains the following governing equations

$$\begin{aligned} N_{1,x_1} + N_{12,x_2} &= 0, \\ N_{12,x_1} + N_{2,x_2} &= 0, \\ M_{1,,x_1}^b + 2M_{12,x_1x_2}^b + M_{2,,x_2}^b - f_e + q &= 0, \\ M_{1,,x_1}^s + 2M_{12,x_1x_2}^s + M_{2,,x_2}^s + S_{13,,x_1}^s + S_{23,,x_2}^s - f_e + q &= 0. \end{aligned} \tag{19}$$

By substituting Eq. (12) into Eq. (10), the governing equations can be expressed in terms of generalized displacements (u, v, w_b, w_s) as

$$\begin{aligned} &A_{11}u_{,x_1x_1} + A_{66}u_{,x_2x_2} + (A_{12}+A_{66})v_{,x_1x_2} \\ &-B_{11}w_{b,x_1x_1x_1} - (B_{12}+2B_{66})w_{b,x_1x_2x_2} \\ &-(B_{12}^s+2B_{66}^s)w_{s,x_1x_2x_2} - B_{11}^s w_{s,x_1x_1x_1} = F_1, \end{aligned} \tag{20a}$$

$$\begin{aligned} &A_{22}v_{,x_2x_2} + A_{66}v_{,x_1x_1} + (A_{12}+A_{66})u_{,x_1x_2} \\ &-B_{22}w_{b,x_2x_2x_2} - (B_{12}+2B_{66})w_{b,x_1x_1x_2} \\ &-(B_{12}^s+2B_{66}^s)w_{s,x_1x_1x_2} - B_{22}^s w_{s,x_2x_2x_2} = F_2, \end{aligned} \tag{20b}$$

$$\begin{aligned}
&B_{11}u_{,x_1x_1x_1}+(B_{12}+2B_{66})u_{,x_1x_2x_2}+(B_{12}+2B_{66})v_{,x_1x_1x_2}+B_{22}v_{,x_2x_2x_2}\\
&-D_{11}w_{b,x_1x_1x_1x_1}-2(D_{12}+2D_{66})w_{b,x_1x_1x_2x_2}-D_{22}w_{b,x_2x_2x_2x_2}\\
&-D_{11}^{s}w_{s,x_1x_1x_1x_1}-2(D_{12}^{s}+2D_{66}^{s})w_{s,x_1x_1x_2x_2}-D_{22}^{s}w_{s,x_2x_2x_2x_2}=F_3,
\end{aligned} \tag{20c}$$

$$\begin{aligned}
&B_{11}^{s}u_{,x_1x_1x_1}+(B_{12}^{s}+2B_{66}^{s})u_{,x_1x_2x_2}+(B_{12}^{s}+2B_{66}^{s})v_{,x_1x_1x_2}\\
&+B_{22}^{s}v_{,x_2x_2x_2}-D_{11}^{s}w_{b,x_1x_1x_1x_1}-2(D_{12}^{s}+2D_{66}^{s})w_{b,x_1x_1x_2x_2}\\
&-D_{22}^{s}w_{b,x_2x_2x_2x_2}-H_{11}^{s}w_{s,x_1x_1x_1x_1}-2(H_{12}^{s}+2H_{66}^{s})w_{s,x_1x_1x_2x_2}\\
&-H_{22}^{s}w_{s,x_2x_2x_2x_2}+A_{55}^{s}w_{s,x_1x_1}+A_{44}^{s}w_{s,x_2x_2}=F_4.
\end{aligned} \tag{20d}$$

Where $\{F\}=\{F_1,F_2,F_3,F_4\}^t$ is generalized force vector.
The components of the generalized force vector $\{F\}$ are given by

$$\begin{aligned}
&F_1=N_{1,x_1}^{T}+N_{1,x_1}^{C}, && F_2=N_{2,x_2}^{T}+N_{2,x_2}^{C},\\
&F_3=f_e+q-\left(M_1^{bT}+M_1^{bC}\right)_{,x_1x_1}-\left(M_2^{bT}+M_2^{bC}\right)_{,x_2x_2},\\
&F_4=f_e+q-\left(M_1^{sT}+M_1^{sC}\right)_{,x_1x_1}-\left(M_2^{sT}+M_2^{sC}\right)_{,x_2x_2}.
\end{aligned} \tag{21}$$

3. Analytical solutions for FGM plates

Following Navier procedure, the sinusoidal external force as well as the transverse sinusoidal temperature and moisture concentration loads presented in the form of double Fourier series as

$$\begin{Bmatrix} q \\ T_k \\ C_k \end{Bmatrix}=\begin{Bmatrix} q_0 \\ t_k \\ c_k \end{Bmatrix}\sin(i\,x_1)\sin(j\,x_2) \qquad (k=1,2,3) \tag{22}$$

Where $i=\pi/a$, $j=\pi/b$, q_0, t_k and c_k are constants and T_k and C_k are defined in Eq. (12).
Following the Navier solution procedure, we assume the following solution form for (u, v, w_b, w_s) that satisfies the simply boundary conditions

$$\begin{Bmatrix} u \\ v \\ w_b \\ w_s \end{Bmatrix}=\begin{Bmatrix} U\cos(i\,x_1)\sin(j\,x_2) \\ V\sin(i\,x_1)\cos(j\,x_2) \\ W_b\sin(i\,x_1)\sin(j\,x_2) \\ W_s\sin(i\,x_1)\sin(j\,x_2) \end{Bmatrix}. \tag{23}$$

Where U, V, W_b, and W_s are arbitrary parameters to be determined subjected to the condition that the solution in Eq. (23) satisfies governing equation (20). Substituting Eq. (23) into Eqs. (20), one obtains

$$[K]\{\Delta\}=\{F\}, \tag{24}$$

and $\{\Delta\} = \{U, V, W_b, W_s\}^t$ and $[K]$ is the symmetric matrix given by

$$[K] = \begin{bmatrix} k_{11} & k_{12} & k_{13} & k_{14} \\ k_{12} & k_{22} & k_{23} & k_{24} \\ k_{13} & k_{23} & k_{33} & k_{34} \\ k_{11} & k_{24} & k_{34} & k_{44} \end{bmatrix}, \tag{25}$$

in which

$$\begin{aligned} k_{11} &= -(A_{11}i^2 + A_{66}j^2), \\ k_{12} &= -i\,j(A_{12} + A_{66}), \\ k_{13} &= i\,[B_{11}i^2 + (B_{12} + 2B_{66}j^2)], \\ k_{14} &= i\,[B_{11}^s i^2 + (B_{12}^s + 2B_{66}^s j^2)], \\ k_{22} &= -(A_{66}i^2 + A_{22}j^2) \\ k_{23} &= j\,[(B_{12} + 2B_{66})i^2 + B_{22}j^2], \\ k_{24} &= j\,[(B_{12}^s + 2B_{66}^s)i^2 + B_{22}^s j^2], \\ k_{33} &= -(D_{11}i^4 + 2(D_{12} + 2D_{66})i^2j^2 + D_{22}j^4 + K + J_1 i^2 + J_2 j^2), \\ k_{34} &= -(D_{11}^s i^4 + 2(D_{12}^s + 2D_{66}^s)i^2j^2 + D_{22}^s j^4 + K + J_1 i^2 + J_2 j^2), \\ k_{44} &= -(H_{11}^s i^4 + 2(H_{11}^s + 2H_{66}^s)i^2j^2 + H_{22}^s j^4 + A_{55}^s i^2 + A_{44}^s j^2 + K + J_1 i^2 + J_2 j^2). \end{aligned} \tag{26}$$

The components of the generalized force vector $\{F\} = \{F_1, F_2, F_3, F_4\}^t$ are given by

$$\begin{aligned} F_1 &= i[(A^T t_1 + B^T t_2 + B_a^T t_3) + (A^C c_1 + B^C c_2 + B_a^C c_3)], \\ F_2 &= j[(A^T t_1 + B^T t_2 + B_a^T t_3) + (A^C c_1 + B^C c_2 + B_a^C c_3)], \\ F_3 &= -q_0 - h(i^2 + j^2)[(B^T t_1 + D^T t_2 + D_a^T t_3) + (B^C c_1 + D^C c_2 + D_a^C c_3)], \\ F_4 &= -q_0 - h(i^2 + j^2)[(B_s^T t_1 + D_s^T t_2 + F_s^T t_3) + (B_s^C c_1 + D_s^C c_2 + F_s^C c_3)]. \end{aligned} \tag{27}$$

Where

$$\{A^T, B^T, D^T\} = \int_{-h/2}^{h/2} \frac{E(x_3)}{1-\nu}\alpha(x_3)\{1,\ \bar{x}_3,\ \bar{x}_3{}^2\}dx_3,$$

$$\{A^C, B^C, D^C\} = \int_{-h/2}^{h/2} \frac{E(x_3)}{1-\nu}\beta(x_3)\{1,\ \bar{x}_3,\ \bar{x}_3{}^2\}dx_3, \tag{28a}$$

$$\{B_a^T, D_a^T\} = \int_{-h/2}^{h/2} \frac{E(x_3)}{1-\nu}\alpha(x_3)\,\overline{\Psi}(x_3)\{1,\ \bar{x}_3\}dx_3,$$

$$\{B_a^C, D_a^C\} = \int_{-h/2}^{h/2} \frac{E(x_3)}{1-\nu}\beta(x_3)\,\overline{\Psi}(x_3)\{1,\ \bar{x}_3\}dx_3, \tag{28b}$$

$$\begin{aligned}\{B_s^T, D_s^T, F_s^T\} &= \int_{-h/2}^{h/2} \frac{E(x_3)}{1-\nu}\alpha(x_3)\bar{f}(x_3)\{1,\ \bar{x}_3,\ \overline{\Psi}(x_3)\}dx_3,\\ \{B_s^C, D_s^C, F_s^C\} &= \int_{-h/2}^{h/2} \frac{E(x_3)}{1-\nu}\beta(x_3)\bar{f}(x_3)\{1,\ \bar{x}_3,\ \overline{\Psi}(x_3)\}dx_3,\end{aligned} \tag{28c}$$

in which $\bar{x}_3 = x_3/h$, and $\overline{\Psi}(x_3) = \frac{1}{\pi}\sin\left(\frac{\pi x_3}{h}\right)$.

4. Discussion of results

In this study, bending analysis of simply supported rectangular FG plates by using the hyperbolic shear deformation plate theory is suggested for investigation. Comparisons are made with available solutions in literature. In order to verify the accuracy of the present analysis, some numerical examples are solved. The first comparison of the power law modeling is given through comparison with elasticity solutions available in literature (Zenkour 2006) and (Reddy 2000) give numerical results for the transverse deflections and stresses in an isotropic plate with power law variation in modulus subject to sinusoidal loading of the form. The material properties of the FGM are indicated in Table 1.

Tables 2 and 3 contain normalized transverse and stresses of a functionally graded square plate with aspect ratio $a/h = 10$. In this study, the numerical results for the mechanical loading is shown in the dimensionless quantities defined as follows

$$\begin{aligned}\bar{u}_3 &= \frac{10h^3E_c}{a^4q_0}u_3\left(\frac{a}{2},\frac{b}{2}\right), \quad \bar{S}_{11} = \frac{h}{aq_0}S_{11}\left(\frac{a}{2},\frac{b}{2},\frac{h}{2}\right)\\ \bar{S}_{12} &= \frac{h}{aq_0}S_{12}\left(0,0,-\frac{h}{3}\right), \quad \bar{S}_{13} = \frac{h}{aq_0}S_{13}\left(0,\frac{b}{2},0\right),\\ K_w &= \frac{k_w a^4}{D}, \quad K_p = \frac{k_p a^2}{D}, \quad D = \frac{Eh^3}{12(1-\nu^2)}.\end{aligned} \tag{29}$$

Results are given for generalized shear deformation theory (Zenkour 2006), higher order shear

Table 1 Material properties used in the FGM plate

Properties	Metal: Titanium, Ti-6Al-4V	Ceramic: Zerconia, ZrO_2
E (GPa)	70	380
ν	0.3	0.3

Table 2 Effects of volume fraction exponent on the dimensionless displacements and stresses of a FGM square plate (a/h = 10, $b = a$ = 1, $K_w = K_p$ = 0, q_0 = 1, $T = C$ = 0)

k	Theory	$\bar{u}_3$	$\bar{S}_{11}$	$\bar{S}_{12}$	$\bar{S}_{13}$
	(Zenkour 2006)	0.2960	1.9955	0.7065	0.2462
Ceramic	Present	0.29604	2.02724	0.70678	0.23215
	% difference	- 0.01351	-1.59057	- 0.03963	5.70674
	(Zenkour 2006)	0.5889	3.0870	0.6110	0.2462
1	Present	0.58893	3.12645	0.61118	0.23215
	% difference	-0.00509	- 1.27793	- 0.02949	5.70674
	(Zenkour 2006)	0.7573	3.6094	0.5441	0.2265
2	Present	0.75718	3.63002	0.54432	0.21190
	% difference	0.01584	- 0.57128	- 0.04043	6.44591
	(Zenkour 2006)	0.8377	3.8742	0.5525	0.2107
3	Present	0.83717	3.86808	0.55278	0.19543
	% difference	0.06326	0.15796	- 0.05067	7.24727
	(Zenkour 2006)	0.8819	4.0693	0.5667	0.2029
4	Present	0.88102	4.03991	0.56710	0.18728
	% difference	0.09978	0.72223	- 0.07058	7.69837
	(Zenkour 2006)	0.9118	4.2488	0.5755	0.2017
5	Present	0.91080	4.20242	0.57585	0.18575
	% difference	0.10967	1.09160	- 0.06081	7.90778
	(Zenkour 2006)	0.9356	4.4244	0.5803	0.2041
6	Present	0.93452	4.36696	0.58075	0.18807
	% difference	0.11543	1.29825	- 0.07754	7.85399
	(Zenkour 2006)	0.9562	4.5971	0.5834	0.2081
7	Present	0.95521	4.53333	0.58378	0.19206
	% difference	0.10353	1.38717	-0.06513	7.70783
	(Zenkour 2006)	0.9750	4.7661	0.5856	0.2124
8	Present	0.97408	4.69925	0.58602	0.19645
	% difference	0.92000	1.40261	- 0.07172	5.56026
	(Zenkour 2006)	0.9925	4.9303	0.5875	0.2164
9	Present	0.99170	4.86294	0.58794	0.20059
	% difference	0.08060	1.36624	- 0.07489	7.30591
	(Zenkour 2006)	1.0089	5.0890	0.5894	0.2198
10	Present	1.00832	5.02282	0.58977	0.20424
	% difference	0.05748	1.30045	- 0.06277	7.07916
	(Zenkour 2006)	1.6070	1.9955	0.7065	0.2462
Metal	Present	1.57882	1.89911	0.70234	0.24229
	% difference	1.75357	4.83036	0.58881	1.58813

Table 3 Effects of volume fraction exponent on the dimensionless displacements and stresses of a FGM square plate (a/h = 10, $b = a$ = 1, $K_w = K_p$ = 0, q_0 = 1, $T = C$ = 0)

k	Theory	$\bar{u}_3$	$\bar{S}_{11}$	$\bar{S}_{12}$	$\bar{S}_{13}$
	HSDT (Reddy 2000)	0.294	1.98915	0.70557	0.23778
Ceramic	Present	0.296044	2.02724	0.706783	0.232158
	% difference	-0.006952	-0.019148	-0.001719	0.023643
	HSDT (Reddy 2000)	0.58895	3.08501	0.61111	0.23817
1	Present	0.588932	3.12645	0.611184	0.232157
	% difference	0.000030	-0.013432	-0.000121	0.025246
	HSDT (Reddy 2000)	0.75747	3.60664	0.54434	0.22568
2	Present	0.757180	3.63002	0.544323	0.211909
	% difference	0.000382	-0.00648	0.000031	0.06102
	HSDT (Reddy 2000)	0.90951	4.24293	0.57368	0.21609
5	Present	0.910803	4.20242	0.575857	0.185754
	% difference	-0.001421	0.04051	-0.003794	0.14038
	HSDT (Reddy 2000)	1.59724	1.98915	0.70557	0.23778
Metal	Present	1.57882	1.89911	0.70234	0.242293
	% difference	0.01153	0.04526	0.00457	-0.01897

deformation theory (Reddy 2000). Results are in good agreement with (Zenkour 2006), whilst in excellent agreement with (Reddy 2000), which is seen by many researchers as a benchmark method (Birman and Byrd 2007, Zhang *et al*. 2012, Thai and Choi 2013).

In the second ccomparison, numerical examples are presented and discussed for verifying the accuracy of the present theory in predicting the bending response of FGM plates under sinusoidal load and a temperature field $T(x_1, x_2, x_3)$ as well as moisture concentration $C(x_1, x_2, x_3)$. The hyperbolic plate theory is presented for small displacement and the corresponding small strains. The material properties of the FGM are considered to be dependent on temperature and moisture. The material properties are taken in the analysis at the reference temperature $T_0 = 25°C$ (room temperature) and moisture concentration $C_0 = 0\%$ as indicate in Table 4.

In this study, the numerical results for the mechanical and hygrothermal loadings are shown in the dimensionless quantities defined as follows

Table 4 Material properties used in the FGM plate

Properties	Metal: Titanium, Ti-6Al-4V	Ceramic: Zerconia, ZrO_2
E (GPa)	66.2	117.0
ν	1/3	1/3
α (10^{-6}/C°)	10.3	7.11
β (10^{-6}/K)	0.33	0

$$\bar{u}_3 = \frac{10^2 D_c}{a^4 q_0} u_3\left(\frac{a}{2}, \frac{b}{2}\right), \quad \bar{S}_{11} = \frac{1}{10^2 q_0} S_{11}\left(\frac{a}{2}, \frac{b}{2}, \frac{h}{2}\right),$$
$$\bar{S}_{12} = \frac{1}{10 q_0} S_{12}\left(0, 0, -\frac{h}{3}\right), \quad \bar{S}_{13} = -\frac{1}{10 q_0} S_{13}\left(0, \frac{b}{2}, 0\right). \tag{30}$$
$$K_w = \frac{k_w a^4}{D}, \quad K_p = \frac{k_p a^2}{D}, \quad D = \frac{E h^3}{12(1-\nu^2)}.$$

Table 5 Effects of volume fraction exponent and elastic foundation parameters on the dimensionless displacements and stresses of a FGM rectangular plate (a/h = 10, b = 3a, q_0 = 100, t_1 = t_3 = 0, t_2 = 10, c_1 = c_3 = 0, c_2 = 100)

k	K_w	K_p	Theory	$\bar{w}$	$\bar{S}_{11}$	$\bar{S}_{12}$	$\bar{S}_{13}$
Ceramic	0	0	Present	1.80709	0.462270	1.55990	−0.41798
			TSDT	1.80712	0.47187	1.55982	−0.42955
			SSDT	1.80708	0.47200	1.55975	−0.44327
	100	0	Present	0.97215	−0.972148	0.852150	−0.01164
			TSDT	0.97216	−0.02740	0.85211	−0.01197
			SSDT	0.97216	−0.02740	0.85211	−0.01235
	0	100	Present	0.18860	−0.48723	0.18797	0.36968
			TSDT	0.18861	−0.49570	0.18806	0.37990
			SSDT	0.18861	−0.49588	0.18810	0.39206
	100	100	Present	0.17309	−0.49633	0.17482	0.37723
			TSDT	0.17309	−0.50498	0.17490	0.38766
			SSDT	0.17309	−0.50716	0.17495	0.40007
0.5	100	100	Present	0.18409	−0.50982	0.18292	0.43981
			TSDT	0.18410	−0.51975	0.18299	0.44334
			SSDT	0.18411	−0.51999	0.18301	0.45728
1	100	100	Present	0.18503	−0.50181	0.15622	0.43334
			TSDT	0.18504	−0.51450	0.15631	0.44545
			SSDT	0.18504	−0.51476	0.15635	0.45984
2	100	100	Present	0.18559	−0.48892	0.13438	0.42571
			TSDT	0.18560	−0.50336	0.13451	0.43831
			SSDT	0.18560	−0.50363	0.13461	0.45337
5	100	100	Present	0.18696	−0.47268	0.12340	0.42443
			TSDT	0.18696	−0.48940	0.12417	0.43754
			SSDT	0.18694	−0.48967	0.12431	0.45322
Metal	100	100	Present	0.18842	−0.42280	0.12011	0.44680
			TSDT	0.18840	−0.43095	0.12087	0.45993
			SSDT	0.18840	−0.43117	0.12092	0.47465

Table 6 Effects of volume fraction exponent and elastic foundation parameters on the dimensionless displacements and stresses of a FGM rectangular plate (a/h = 10, b = 3a, q_0 = 100, t_1 = 0, t_2 = t_3 = 10, c_1 = 0, c_2 = c_3 = 100)

k	K_w	K_p	Theory	$\bar{w}$	$\bar{S}_{11}$	$\bar{S}_{12}$	$\bar{S}_{13}$
Ceramic	0	0	Present	2.54076	0.51588	2.20381	−0.41354
			TSDT	2.54076	0.52522	2.20374	−0.42454
			SSDT	2.54068	0.52552	2.20366	−0.43753
	100	0	Present	1.36683	−0.17281	1.20872	0.15777
			TSDT	1.36682	−0.17643	1.20877	0.16257
			SSDT	1.36680	−0.17649	1.20881	0.16834
	0	100	Present	0.26517	−0.81910	0.27488	0.69390
			TSDT	0.26518	−0.83500	0.27507	0.71354
			SSDT	0.26518	−0.83531	0.27519	0.73692
	100	100	Present	0.24336	−0.83190	0.25639	0.70452
			TSDT	0.24336	−0.84804	0.25658	0.72442
			SSDT	0.24337	−0.84835	0.25670	0.74816
0.5	100	100	Present	0.26194	−0.86236	0.28023	0.75161
			TSDT	0.26195	−0.87239	0.28034	0.81947
			SSDT	0.26196	−0.87282	0.28041	0.84586
1	100	100	Present	0.26330	−0.83867	0.23741	0.79871
			TSDT	0.26330	−0.86205	0.23762	0.82148
			SSDT	0.26330	−0.86252	0.23772	0.84866
2	100	100	Present	0.26396	−0.81483	0.20107	0.78289
			TSDT	0.26396	−0.84138	0.20133	0.80652
			SSDT	0.26395	−0.84185	0.20154	0.83484
5	100	100	Present	0.26603	−0.78678	0.18423	0.77849
			TSDT	0.26601	−0.81745	0.18459	0.80297
			SSDT	0.26600	−0.81792	0.18486	0.83230
Metal	100	100	Present	0.26729	−0.77772	0.18167	0.79866
			TSDT	0.26774	−0.71656	0.18286	0.84003
			SSDT	0.26775	−0.71694	0.18298	0.86748

Numerical results are tabulated in Tables 5 and 6 using the present four variable refined plate theory. The correlation between the present four variable refined plate theory and different higher-order shear deformation theories is illustrated in Tables 5 and 6. These tables give also the effects of the volume fraction exponent ratio k and elastic foundation on the dimensionless deflection and stresses of FGM rectangular plate, including the effect of the temperature and moisture fields. The obtained results are compared with those predicted by SSDT and TSDT. An excellent agreement is obtained between the present theory and TSDT for all values of power law index k and with or without the presence of the elastic foundation. It is important to observe that the

stresses for a fully ceramic plate are not the same as that for a fully metal plate with elastic foundations. This is because the plate here is affected with the inclusion of the temperature field. The number of primary variables in this theory is even less than that of higher-order shear deformation plate theories. The theory gives parabolic distribution of transverse shear strains, and satisfies the zero traction boundary conditions on the surfaces of the plate without using shear correction factors. It can be concluded that the present theory is not only accurate but also comparatively simple and quite elegant in predicting the hygro-thermo-mechanical bending response of FGM plates resting on Winkler's or Pasternak's elastic foundations.

Figs. 2 and 3 show the variation of the dimensionless center deflection $\bar{u}_3$ with the side-to-thickness a/h and plate aspect ratios b/a, respectively. The deflection is maximum for the metallic plate and minimum for the ceramic plate irrespective of the values of temperature, moisture, and elastic foundation parameters. It is evident that the FGM plates deflection falls somewhere between the deflections of pure metal and pure ceramic plates. In addition, the deflection is increasing in the absence of the foundations and the effect of moisture parameter may be less than that of the temperature one.

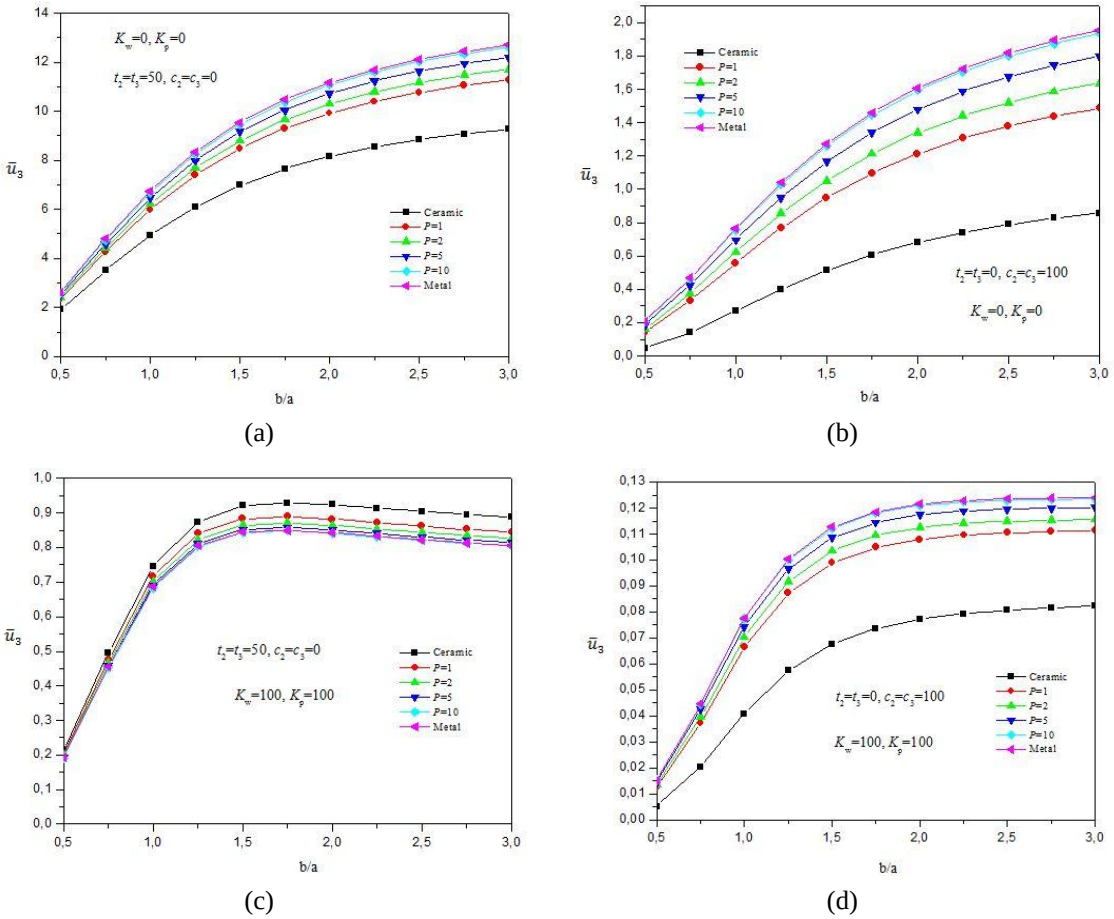

Fig. 2 Dimensionless center deflection $\bar{u}_3$ versus plate aspect ratio b/a for FGM plate on Winkler-Pasternak foundations

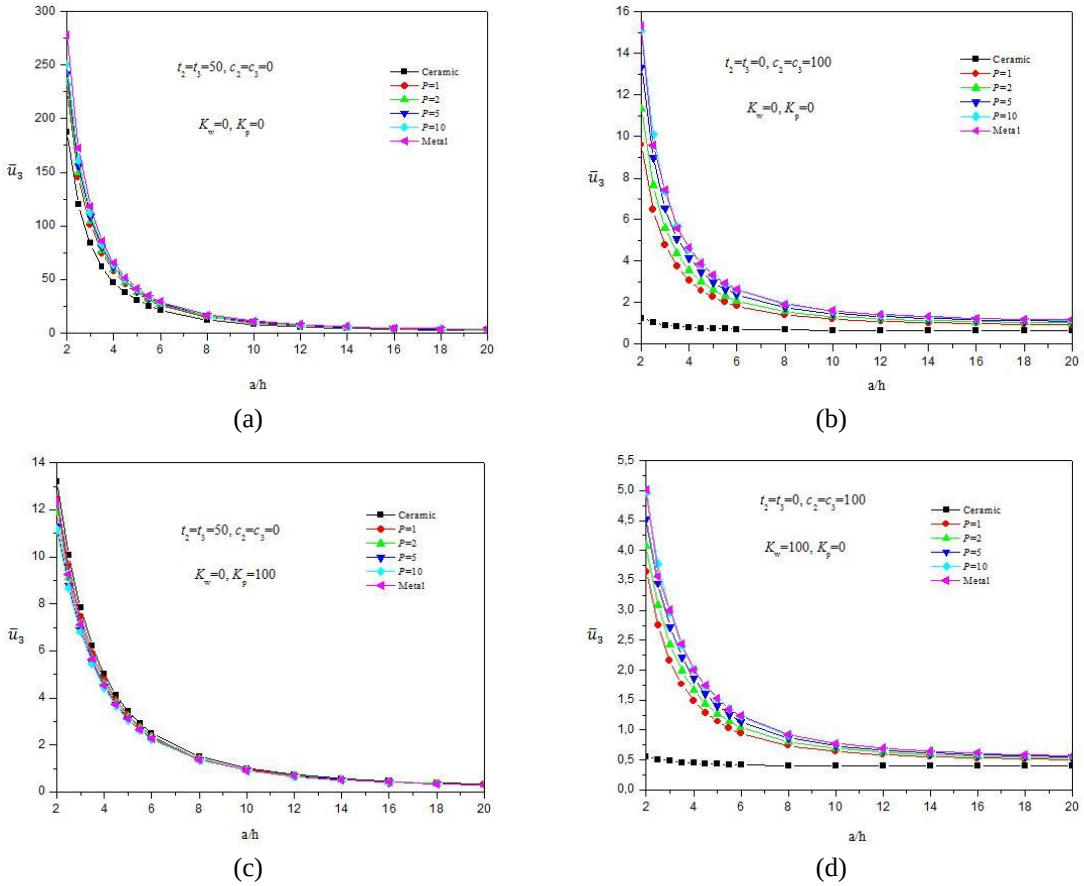

Fig. 3 Dimensionless center deflection $\bar{u}_3$ versus side-to-thickness ratio a/h for FGM plate on Winkler-Pasternak foundations

All examples have been solved numerically using sinusoidal distribution field $\bar{\Psi}(x_3)$ in the third term of temperature and moisture expressions Eqs. (12). In this study, three different distributions fields of temperature and moisture (cubic, sinusoidal and exponential) are used respectively as follows

$$\bar{\Psi}(x_3) = z\left(1-\left(\frac{4}{3}\right)\left(\frac{x_3}{h}\right)^2\right)$$
$$\bar{\Psi}(x_3) = \frac{h}{\pi}\sin\left(\frac{\pi x_3}{h}\right) \tag{31}$$
$$\bar{\Psi}(x_3) = x_3\, e^{-2\left(\frac{x_3}{h}^2\right)}$$

Figs. 4 and 6 depict the through-the-thickness distributions of the non-dimensional axial stress S_{11}, longitudinal tangential S_{12} and transversal shear (S_{13}) in the rectangular FGM plates on elastic foundations for different values of moistures and temperatures respectively. In this figures, it is assumed, that q_0 = 100 GPa, a/h = 10, b/a = 3, k = 2. As exhibited in Figs. 4 and 5, the *maximum*

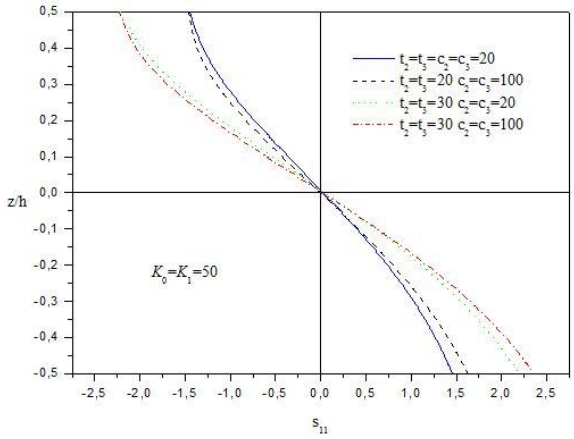

Fig. 4 Variation of dimensionless in-plane longitudinal stress (S_{11}) through the thickness of a rectangular FGM plate on elastic foundations for different values of moistures and temperatures

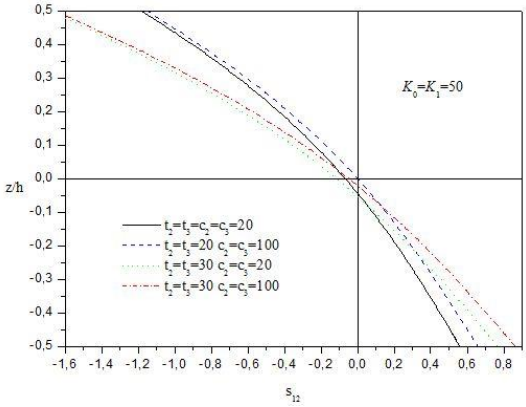

Fig. 5 Variation of dimensionless longitudinal tangential stress (S_{12}) through the thickness of a rectangular FGM plate on elastic foundations for different values of moistures and temperatures

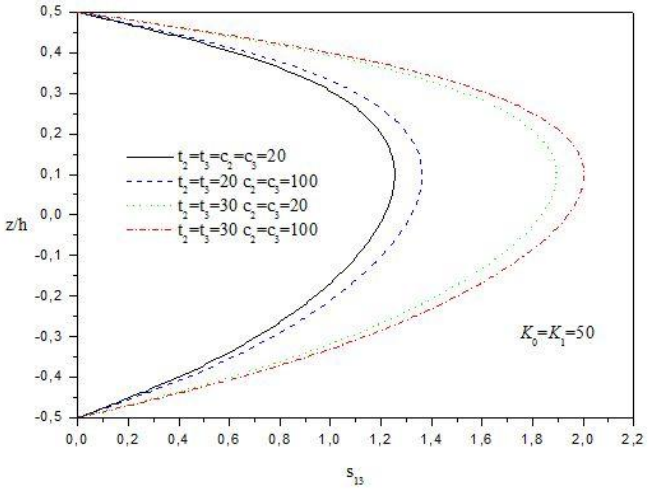

Fig. 6 Variation of dimensionless transversal shear stress (S_{13}) through the thickness of rectangular FGM plate on elastic foundations for different values of moistures and temperatures

compressive stresses occur at a point on the top surface and the maximum tensile stresses occur, of course, at a point on the bottom surface of the FGM plates. It can be seen that the shear stresses increase with the increase of both thermal and moisture load, and the maximum value occurs at a point above the mid-plane of the FGM plate.

Figs. 7 to 10 show the relation between the dimensionless center deflection $\bar{u}_3$, the axial stress $\bar{S}_{11}$, the longitudinal tangential stress $\bar{S}_{12}$, the transversal shear stress $\bar{S}_{13}$ and the plate aspect ratio b/a for three different distributions fields of temperature and moisture. All results of the dimensionless center deflection $\bar{u}_3$, the axial stress $\bar{S}_{11}$, the longitudinal tangential stress $\bar{S}_{12}$ and

the transversal shear stress $\bar{S}_{13}$ are similar values with a difference percent of 1.5. Furthermore, the sinusoidal distribution field gives intermediate value in deflection and stresses cases. The cubic distribution field gives higher values relatively than those of the other two distributions fields in the deflection and longitudinal tangential stress cases. In contrast with axial and transversal shear stress cases, the exponential distribution gives higher values relatively than those of the other two distributions.

The relation between the dimensionless center deflection $\bar{u}_3$, the axial stress $\bar{S}_{11}$, the longitudinal tangential stress $\bar{S}_{12}$, the transversal shear stress $\bar{S}_{13}$ and the plate aspect ratio b/a for different E_m/E_c with or without hygrothermal effects are illustrated in Figs. 11 to 18. The deflection, the axial and the transversal shear stress increase upon increasing the plate aspect ratio b/a, the deflection , axial and transversal shear stress are maximum for $E_m/E_c = 0.03$ and

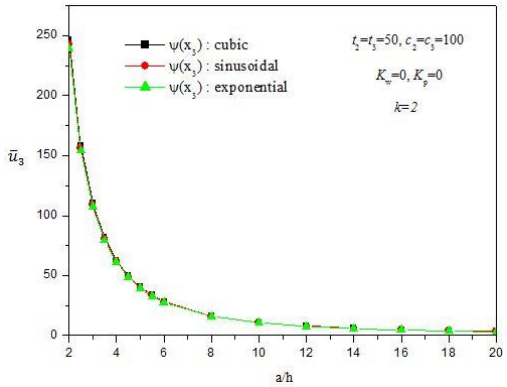

Fig. 7 Dimensionless center deflection $\bar{u}_3$ versus side-to-thickness ratio a/h for FGM rectangular plate for different distributions of $\Psi(x_3)$

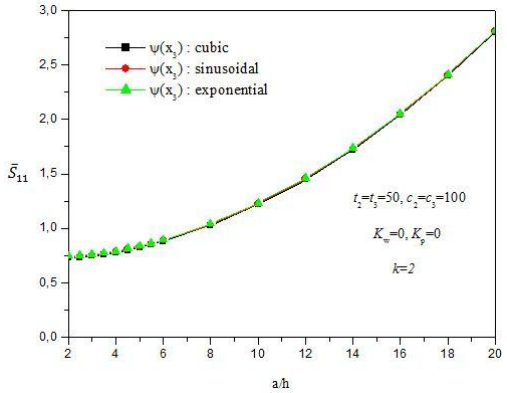

Fig. 8 Dimensionless axial stress $\bar{S}_{11}$ versus side-to-thickness ratio a/h for FGM rectangular plate for different distributions of $\Psi(x_3)$

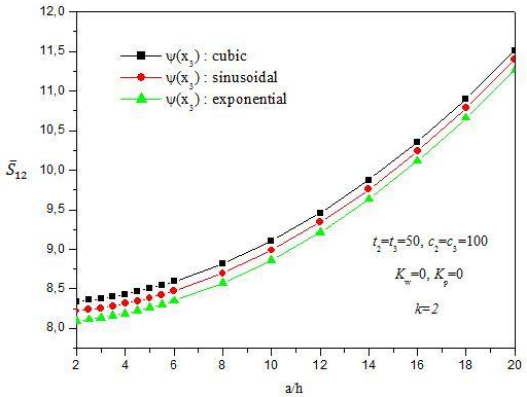

Fig. 9 Dimensionless longitudinal tangential stress $\bar{S}_{12}$ versus side-to-thickness ratio a/h for FGM rectangular plate for different distributions of $\Psi(x_3)$

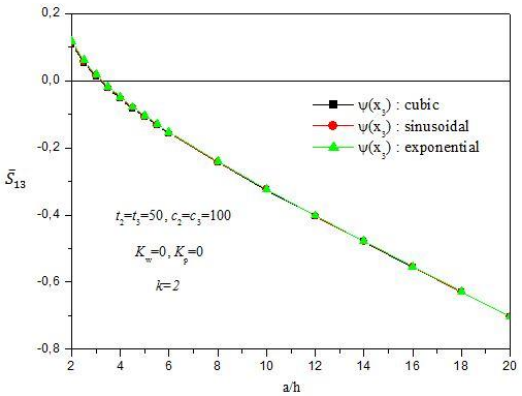

Fig. 10 Dimensionless transversal shear stress $\bar{S}_{13}$ versus side-to-thickness ratio a/h for FGM rectangular plate for different distributions of $\Psi(x_3)$

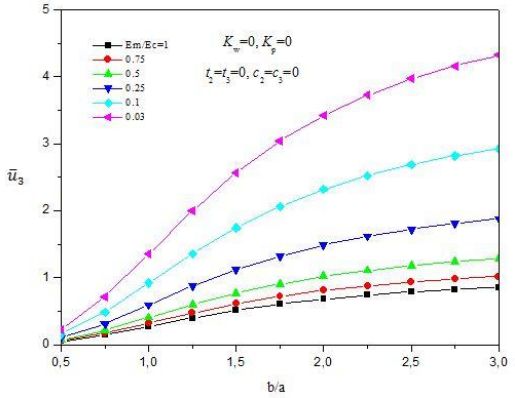

Fig. 11 Dimensionless center deflection $\bar{u}_3$ versus plate aspect ratio b/a for FGM plate for different E_m/E_c ratios ($k = 2, a/h = 10$)

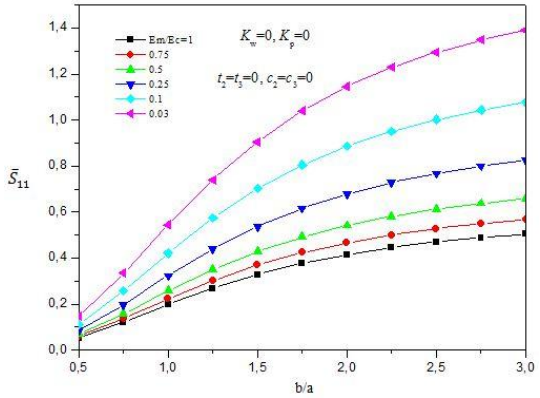

Fig. 12 Dimensionless axial stress $\bar{S}_{11}$ versus plate aspect ratio b/a for FGM plate for different E_m/E_c ratios ($k = 2, a/h = 10$)

minimum for $E_m/E_c = 1$ as shown in Figs. 11, 12, 14 to 16 and 18. In the case of without hygrothermal effects, the longitudinal tangential stress increases upon increasing the aspect ratio for b/a less than 1.75. However, when b/a is greater than 1.75 the longitudinal tangential stress decreases upon increasing the aspect ratio as shown in Fig. 13. In the case of with hygrothermal effects, the longitudinal tangential stress increases upon increasing the aspect ratio for b/a less than 1.0. However, when b/a is greater than 1.0 the longitudinal tangential stress decreases upon increasing the aspect ratio. In both cases with or without hygrothermal effects, the longitudinal tangential stress is maximum for $E_m/E_c = 1$ and minimum for $E_m/E_c = 0.03$ as shown in Figs. 13 and 17.

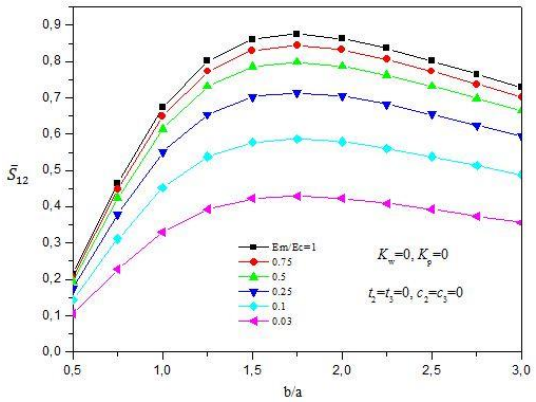

Fig. 13 Dimensionless longitudinal tangential stress $\bar{S}_{12}$ versus plate aspect ratio b/a for FGM plate for different E_m/E_c ratios ($k = 2, a/h = 10$)

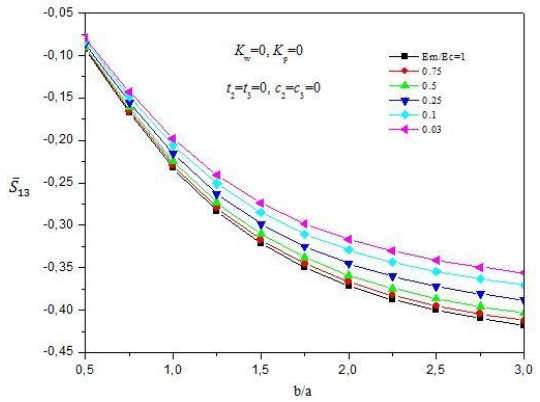

Fig. 14 Dimensionless transversal shear stress $\bar{S}_{13}$ versus plate aspect ratio b/a for FGM plate for different E_m/E_c ratios ($k = 2, a/h = 10$)

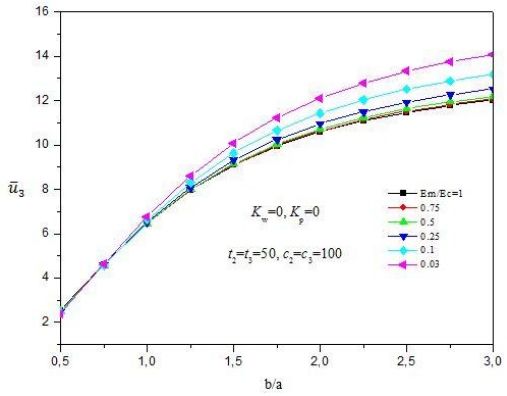

Fig. 15 Dimensionless center deflection $\bar{u}_3$ versus plate aspect ratio b/a for FGM plate for different E_m/E_c ratios $(k = 2, a/h = 10)$

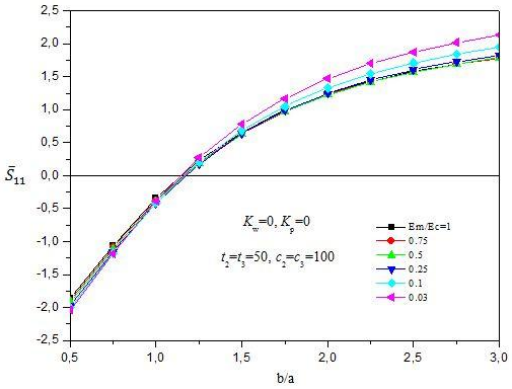

Fig. 16 Dimensionless axial stress $\bar{S}_{11}$ versus plate aspect ratio b/a for FGM plate for different E_m/E_c ratios $(k = 2, a/h = 10)$

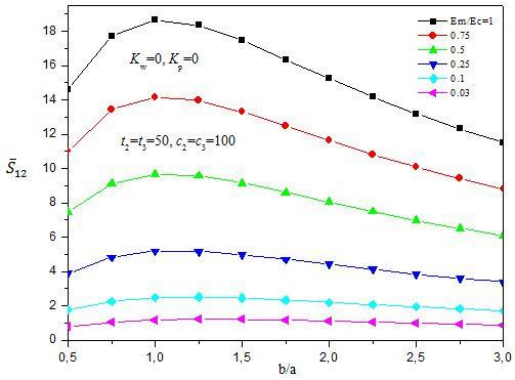

Fig. 17 Dimensionless longitudinal tangential stress $\bar{S}_{12}$ versus plate aspect ratio b/a for FGM plate for different E_m/E_c ratios $(k = 2, a/h = 10)$

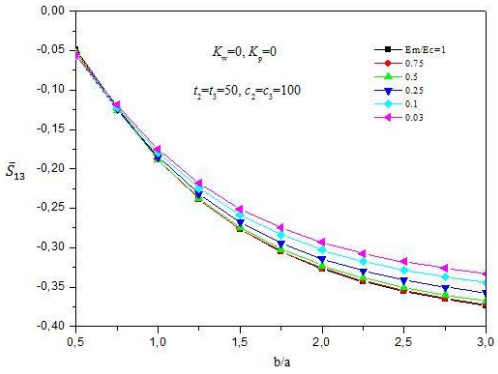

Fig. 18 Dimensionless transversal shear stress $\bar{S}_{13}$ versus plate aspect ratio b/a for FGM plate for different E_m/E_c ratios $(k = 2, a/h = 10)$

5. Conclusions

The paper presents thermo-mechanical behaviors of the FGM plate in hygrothermal environmental conditions are studied. The plate is described and discussed according to the hyperbolic shear deformation theory. The present analysis includes the effects of temperature and moisture concentration on the material properties.

Dimensionless displacements and stresses are computed for plates with ceramic-metal mixture.

Illustrating examples are carried out, with the most important conclusions that the effects of moisture concentration parameter on thermo-mechanical responses of the FG plates are considerably different. The influence of moisture concentration as well as other parameter is highly significant. The bending response of the FG plate deteriorates considerably with the increase in temperature and moisture concentration.

Some general observations of this study can be summarized as follows:

- The deflection is maximum for the metallic plate and minimum for the ceramic plate irrespective of the values of temperature, moisture, and elastic foundation parameters. It is evident that the FGM plates deflection falls somewhere between the deflections of pure metal and pure ceramic plates. In addition, the deflection is increasing in the absence of the foundations and the effect of moisture parameter may be less than that of the temperature one.
- All results of the dimensionless center deflection $\bar{u}_3$, the axial stress $\bar{S}_{11}$, the longitudinal tangential stress $\bar{S}_{12}$ and the transversal shear stress $\bar{S}_{13}$ are similar values with a difference percent of 1.5. Furthermore, the sinusoidal distribution field gives intermediate value in deflection and stresses cases. The cubic distribution field gives higher values relatively than those of the other two distributions fields in the deflection and longitudinal tangential stress cases. In contrast with axial and transversal shear stress cases, the exponential distribution gives higher values relatively than those of the other two distributions.
- The relation between the dimensionless center deflection $\bar{u}_3$, the axial stress $\bar{S}_{11}$, the longitudinal tangential stress $\bar{S}_{12}$, the transversal shear stress $\bar{S}_{13}$ and the plate aspect ratio b/a for different E_m/E_c with or without hygrothermal effects are illustrated in Figs. 11 to 18. The deflection, the axial and the transversal shear stress increase upon increasing the plate aspect ratio b/a, the deflection , axial and transversal shear stress are maximum for $E_m/E_c = 0.03$ and minimum for $E_m/E_c = 1$ as shown in Figs. 11, 12, 14 to 16 and 18. In the case of without hygrothermal effects, the longitudinal tangential stress increases upon increasing the aspect ratio for b/a less than 1.75. However, when b/a is greater than 1.75 the longitudinal tangential stress decreases upon increasing the aspect ratio as shown in Fig. 13. In the case of with hygrothermal effects, the longitudinal tangential stress increases upon increasing the aspect ratio for b/a less than 1.0. However, when b/a is greater than 1.0 the longitudinal tangential stress decreases upon increasing the aspect ratio. In both cases with or without hygrothermal effects, the longitudinal tangential stress is maximum for $E_m/E_c = 1$ and minimum for $E_m/E_c = 0.03$ as shown in Figs. 13 and 17.

References

Ait Amar Meziane, M., Abdelaziz, H.H. and Tounsi, A. (2014), "An efficient and simple refined theory for buckling and free vibration of exponentially graded sandwich plates under various boundary conditions", *J. Sandw. Struct. Mater.*, **16**(3), 293-318.

Ait Atmane, H., Tounsi, A. and Bernard, F. (2016), "Effect of thickness stretching and porosity on mechanical response of a functionally graded beams resting on elastic foundations", *Int. J. Mech. Mater. Des.* [In Press]

Ait Yahia, S., Ait Atmane, H., Houari, M.S.A. and Tounsi, A. (2015), "Wave propagation in functionally graded plates with porosities using various higher-order shear deformation plate theories", *Struct. Eng. Mech., Int. J.*, **53**(6), 1143-1165.

Bahrami, A. and Nosier, A. (2007), "Interlaminar hygrothermal stresses in laminated plates", *Int. J. Solids Struct.*, **44**(25-26), 8119-8142.

Belabed, Z., Houari, M.S.A., Tounsi, A., Mahmoud, S.R. and Anwar Bég, O. (2014), "An efficient and simple higher order shear and normal deformation theory for functionally graded material (FGM) plates", *Composites*: *Part B*, **60**, 274-283.

Benachour, A., Tahar, H.D., Ait Atmane, H., Tounsi, A. and Meftah, S.A. (2011), "A four variable refined plate theory for free vibrations of functionally graded plates with arbitrary gradient", *Composites, Part B*, **42**(6), 1386-1394.

Bennoun, M., Houari, M.S.A. and Tounsi, A. (2016), "A novel five variable refined plate theory for vibration analysis of functionally graded sandwich plates", *Mech. Adv. Mater. Struct.*, **23**(4), 423-431.

Benkhedda, A., Tounsi, A. and Adda bedia, E.A. (2008), "Effect of temperature and humidity on transient hygrothermal stresses during moisture desorption in laminated composite plates", *Compos. Struct.*, **82**(4), 629-635.

Bessaim, A., Houari, M.S.A., Tounsi, A., Mahmoud, S.R. and Adda Bedia, E.A. (2013), "A new higher-order shear and normal deformation theory for the static and free vibration analysis of sandwich plates with functionally graded isotropic face sheets", *J. Sandw. Struct. Mater.*, **15**(6), 671-703.

Birman, V. and Byrd, L.W. (2007), "Modeling and analysis of functionally graded materials and structures", *Appl. Mech. Rev.*, **60**(1-6), 195-216.

Bouchafa, A., Bachir Bouiadjra, M., Houari, M.S.A. and Tounsi, A. (2015), "Thermal stresses and deflections of functionally graded sandwich plates using a new refined hyperbolic shear deformation theory", *Steel Compos. Struct., Int. J.*, **18**(6), 1493-1515.

Bouderba, B., Houari, M.S.A. and Tounsi, A. (2013), "Thermomechanical bending response of FGM thick plates resting on Winkler–Pasternak elastic foundations", *Steel Compos. Struct., Int. J.*, **14**(1), 85-104.

Bourada, M., Tounsi, A., Houari, M.S.A. and Adda Bedia, E.A. (2012), "A new four-variable refined plate theory for thermal buckling analysis of functionally graded sandwich plates", *J. Sandw. Struct. Mater.*, **14**(1), 5-33.

Bourada, M., Kaci, A., Houari, M.S.A. and Tounsi, A. (2015), "A new simple shear and normal deformations theory for functionally graded beams", *Steel Compos. Struct., Int. J.*, **18**(2), 409-423.

Bousahla, A.A., Houari, M.S.A., Tounsi, A. and Adda Bedia, E.A. (2014), "A novel higher order shear and normal deformation theory based on neutral surface position for bending analysis of advanced composite plates", *Int. J. Comput. Method.*, **11**(6), 1350082.

Dai, K.Y., Liu, G.R., Han, X. and Lim, K.M. (2005), "Thermomechanical analysis of functionally graded material (FGM) plates using element-free Galerkin method", *Comput. Struct.*, **83**(17-18), 1487-1502.

Fekrar, A., Houari, M.S.A., Tounsi, A. and Mahmoud, S.R. (2014), "A new five-unknown refined theory based on neutral surface position for bending analysis of exponential graded plates", *Meccanica*, **49**(4), 795-810.

Hamidi, A., Houari, M.S.A., Mahmoud, S.R. and Tounsi, A. (2015), "A sinusoidal plate theory with 5-unknowns and stretching effect for thermomechanical bending of functionally graded sandwich plates", *Steel Compos. Struct., Int. J.*, **18**(1), 235-253.

Hebali, H., Tounsi, A., Houari, M.S.A., Bessaim, A. and Adda Bedia, E.A. (2014), "A new quasi-3D hyperbolic shear deformation theory for the static and free vibration analysis of functionally graded plates", *ASCE J. Eng. Mech.*, **140**(2), 374-383.

Houari, M.S.A., Tounsi, A. and Anwar Bég, O. (2013), "Thermoelastic bending analysis of functionally graded sandwich plates using a new higher order shear and normal deformation theory", *Int. J. Mech. Sci.*, **76**, 467-479.

Javaheri, R. and Eslami, M.R. (2002), "Thermal buckling of functionally graded plates", *AIAA J.*, **40** 162-168.

Khalfi, Y., Houari, M.S.A. and Tounsi, A. (2014), "A refined and simple shear deformation theory for thermal buckling of solar functionally graded plates on elastic foundation", *Int. J. Comput. Method.*, **11**(5), 1350077.

Koizumi, M. (1993), "The concept of FGM, ceramic transactions", *Function. Grad. Mater.*, **34**, 3-10.

Liu, G.R. and Tani, J. (1994), "Surface-waves in functionally gradient piezoelectric plates", *J. Vib. Acoust.*, **116**(4), 440-448.

Liu, G.R., Han, X. and Lam, K.Y. (1999), "Stress waves in functionally gradient materials and its use for material characterization", *Compos. Part B-Eng.*, **30**(4), 383-394.

Liu, G.R., Han, X. and Lam, K.Y. (2001), "An integration technique for evaluating confluent

hypergeometric functions and its application to functionally graded materials", *Comput. Struct.*, **79**(10), 1039-1047.
Liu, G.R., Dai, K.Y., Han, X. and Ohyoshi, T. (2003), "Dispersion of waves and characteristic wave surfaces in functionally graded piezoelectric plates", *J. Sound Vib.*, **268**(1), 131-147.
Lo, S.H., Zhen, W., Cheung, Y.K. and Wanji, C. (2010), "Hygrothermal effects on multilayered composite plates using a refined higher order theory", *Compos. Struct.*, **92**(3), 633-646.
Mahi, A., Adda Bedia, E.A. and Tounsi, A. (2015), "A new hyperbolic shear deformation theory for bending and free vibration analysis of isotropic, functionally graded, sandwich and laminated composite plates", *Appl. Math. Model.*, **39**(9), 2489-2508.
Patel, B.P., Ganapathi, M. and Makhecha, D.P. (2002), "Hygrothermal effects on the structural behavior of thick composite laminates using higher-order theory", *Compos. Struct.*, **56**(1), 25-34.
Rao, V.V.S. and Sinha, P.K. (2004), "Bending characteristic of thick multidirectional composite plates under hygrothermal environment", *J. Reinf. Plast. Compos.*, **23**(14), 1481-1495.
Reddy, J.N. (2000), "Analysis of functionally graded plates", *Int. J. Numer. Method. Eng.*, **47**(1-3), 663-684.
Said, A., Ameur, M., Bousahla, A.A. and Tounsi, A. (2014), "A new simple hyperbolic shear deformation theory for functionally graded plates resting on Winkler-Pasternak elastic foundations", *Int. J. Comput. Methods*, **11**(6), 1350098.
Shen, H.S. (2001), "Hygrothermal effects on the postbuckling of shear deformable laminated plates", *Int. J. Mech. Sci.*, **43**(5), 1259-1281.
Suresh, S. and Mortensen, A. (1998), *Fundamentals of Functionally Graded Materials*, Institute of Materials (IOM) Communications Limited, London, UK.
Tani, J. and Liu, G.R. (1993), "SH surface-waves in functionally gradient piezoelectric plates", *JSME Int. J Series A-Mech. Mater. Eng.*, **36**(2), 152-155.
Thai, H.T. and Choi, D.H. (2013), "A simple first-order shear deformation theory for the bending and free vibration analysis of functionally graded plates", *Compos. Struct.*, **101**, 332-340.
Tounsi, A., Houari, M.S.A., Benyoucef, S. and Adda Bedia, E.A. (2013), "A refined trigonometric shear deformation theory for thermoelastic bending of functionally graded sandwich plates", *Aerosp. Sci. Technol.*, **24**(1), 209-220.
Wang, X., Dong, K. and Wang, X.Y. (2005), "Hygrothermal effect on dynamic interlaminar stresses in laminated plates with piezoelectric actuators", *Compos. Struct.*, **71**(2), 220-228.
Whitney, J.M. and Ashton, J.E. (1971), "Effect of environment on the elastic response of layered composite plates", *AIAA J.*, **9**(9), 1708-1713.
Zenkour, A.M. (2006), "Generalized shear deformation theory for bending analysis of functionally graded plates", *Appl. Math. Model.*, **30**(1), 67-84.
Zenkour, A.M. (2010), "Hygro-thermo-mechanical effects on FGM plates resting on elastic foundations", *Compos. Struct.*, **93**, 234-238.
Zhang, W., Hao, Y.X. and Yang, J. (2012), "Nonlinear dynamics of FGM circular cylindrical shell with clamped–clamped edges", *Compos. Struct.*, **94**(3), 1075-1086.
Zidi, M., Tounsi, A., Houari, M.S.A., Adda Bedia, E.A. and Anwar Bég, O. (2014), "Bending analysis of FGM plates under hygro-thermo-mechanical loading using a four variable refined plate theory", *Aerosp. Sci. Technol.*, **34**, 24-34.

CC